Complete Urban Surface Temperatures

J. A. VOOGT* AND T. R. OKE

Department of Geography, University of British Columbia, Vancouver, British Columbia, Canada

(Manuscript received 16 September 1996, in final form 20 February 1997)

ABSTRACT

An observation program using ground and airborne thermal infrared radiometers is used to estimate the surface temperature of urban areas, taking into account the total active surface area. The authors call this the complete urban surface temperature. This temperature is not restricted by the viewing biases inherent in remote sensors used to estimate surface temperature over rough surfaces such as cities. Two methods to estimate the complete surface temperature are presented. Results for three different land-use areas in the city of Vancouver, British Columbia, Canada, show significant differences exist between the complete, nadir, and off-nadir airborne estimates of urban surface temperature during daytime. For the sites and times studied, the complete surface temperature is shown to agree with airborne off-nadir estimates of the apparent surface temperature of the most shaded walls. Some implications of using the complete surface temperature to estimate screen level air temperature and to calculate surface sensible heat flux are given.

1. Introduction

Surface temperature is an important boundary condition for studies of the urban atmosphere. Its measurement in cities is difficult because of the complex structure of the urban–atmosphere interface. Furthermore, there are strong microscale variations of surface temperature that arise due to changes in radiant load with surface slope and aspect, shading, and variations in surface thermal and radiative properties.

Studies of single urban canyons have used in situ thermocouple or thermistor thermometry to estimate surface temperatures. An alternative is to use infrared radiometry, where instruments indirectly estimate an apparent surface temperature based upon the radiance received from that area of the surface that lies within the instrument's instantaneous field of view (FOV). An advantage of this approach is better spatial sampling over the microscale temperature variations that occur across an individual building facet. Such instruments can be used in single canyons or mounted on a vehicle to extend the scale of observation (Voogt 1995).

Thermal infrared radiometry from aircraft or satellite platforms has often been advocated as a means of providing more spatially representative measurements of surface temperature over larger areas of cities than is feasible using ground-based studies. However, studies over ''rough'' natural and agricultural surfaces (e.g., Boissard et al. 1990; Paw U 1992) demonstrate that directional variations of thermal emittance (which may be termed *effective anisotropy*) pose difficulties in the interpretation of the results.

Roth et al. (1989) suggested that urban areas may be prone to similar effects. Work by Voogt (1995) confirms the existence of strong effective anisotropy in thermal emittance at the land-use scale (10^2–10^6 m^2) over urban areas. Remotely sensed urban surface temperatures are subject to strong variations due to viewing restrictions of the urban surface structure by the instrument and differential heating patterns created by sun-surface geometric configuration. These results imply that remote sensors undersample the urban surface.

In this paper, we combine surface temperature observations obtained using infrared radiometry from different observation platforms with surface structural information to produce an urban surface temperature that better takes into account the temperatures of all the surfaces present. We term this temperature the *complete (urban) surface temperature* T_c. Complete surface temperatures are compared with remotely sensed surface temperatures of urban areas to assess the degree to which remotely measured estimates of urban surface temperature differ from the temperature of the entire three-dimensional surface.

2. Definitions

a. The complete urban surface

From a climatological perspective, the surface is critically important. It is where the principal sources and

* Current affiliation: Department of Geography, University of Western Ontario, London, Ontario, Canada.

Corresponding author address: Dr. James A. Voogt, Dept. of Geography, University of Western Ontario, London, ON N6A 5C2, Canada.
E-mail: voogt@sscl.uwo.ca

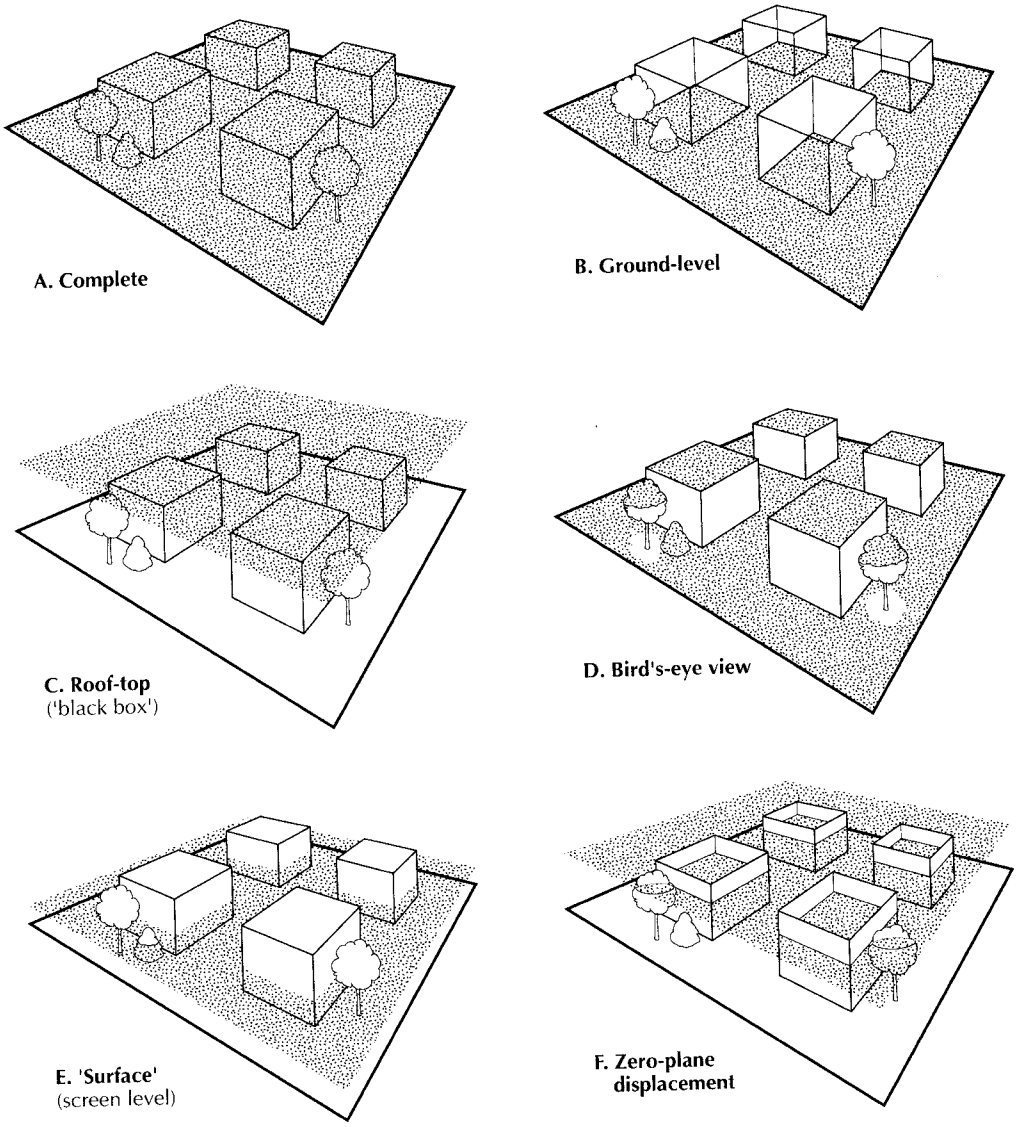

FIG. 1. Schematic illustration of different definitions of the urban surface. (a) Complete, (b) ground level, (c) rooftop equivalent (''black box''), (d) bird's-eye view, (e) ''surface'' (screen level) observed, and (f) zero-plane displacement.

sinks of heat, mass, and momentum are located. Properties of the surface control the partitioning and conversion of these entities, so the nature of the surface strongly conditions the behavior of the lowest layers of the atmosphere. Specification of surface properties and conditions is thus an important objective for study and a necessary prerequisite to gain understanding of the climate system. If the relatively young field of urban climatology is to gain insight, it has to grapple with definition and specification of the heterogeneous and highly convoluted three-dimensional urban–atmosphere interface.

Surface representations in boundary layer meteorology simplify and approximate the actual nature of the surface (Fig. 1). What is required is the complete area comprising the boundary between the surface system and the air (Fig. 1a). Often what is used is the surface ''seen'' by a sensor. For example: a plane at the ground (Fig. 1b) or above roof level (Fig. 1c) that ignores the canopy or treats it as a ''black box''; a bird's-eye view of an infrared thermometer placed above the system (Fig. 1d); planes of observation that coincide with the measurement level of a sensor, such as a screen-level thermometer to measure the air temperature (Fig. 1e); or a plane at some intermediate height in the canopy, which represents an effective surface, usually for the purpose of modeling the integrated system (Fig. 1f).

The surface representation adopted generally is scale dependent; details of the surface structure are increasingly simplified as the total area increases.

TABLE 1. Definition of area component symbols.

Symbol	Description
A_p	Plan (horizontal) area (obtained from map or aerial photo)
A_o	Horizontal ground-level area (grass, roads, gardens)
A_r	Roof area (actual)
A_{pr}	Plan or apparent roof area: for flat roofs $A_r = A_{pr}$; equivalent to building plan area
A_w	Wall area (total or with an additional subscript denoting facet direction)
A_b	Building area (sum of roof and wall areas)
A_v	Vegetation area (three-dimensional tree representation)
A_{pv}	Plan or apparent vegetation area (horizontal projection), subdivided into trees with trunk heights ($h_{tk} = 0, >0$)
A_c	Complete surface area

The surface representation adopted here includes major structural features such as buildings and trees (or sizable shrubs). In general, the surface representation does not include details at length scales less than that of a building or tree. Landform relief is ignored. Component areas are listed in Table 1 and shown schematically in Fig. 2.

b. The complete urban surface temperature

The complete urban surface temperature T_c is an area-weighted temperature. Component surface temperatures may be combined in proportion to their areal fraction of the complete surface. The complete surface longwave emission L_c may be written

$$L_c = \sum_{i=1}^{n} f_i L_i, \tag{1}$$

where f_i are the fractional areas with emission L_i. An equivalent radiant temperature may be calculated from (1) assuming blackbody emission and using the Stefan–Boltzmann law or other temperature-emittance relations defined for particular spectral regions (e.g., Singh 1985), depending upon the characteristics of the instruments used to obtain L_i. Heilman et al. (1981), Kustas et al. (1990), and Sun and Mahrt (1995) have used similar definitions to describe a composite temperature that they use to represent the apparent temperature of the surface as observed (rather than the complete surface) by a thermal remote sensor.

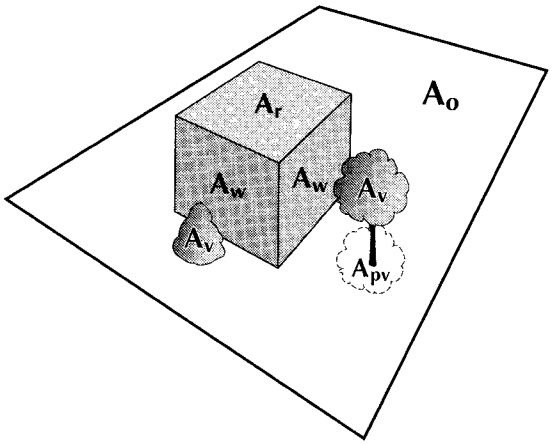

FIG. 2. Illustration of component areas composing a typical urban building unit.

To obtain L_c from (1) requires the specification of surface classes, their representative temperatures, and the fractional area of each surface class. While this procedure can be implemented for agricultural crops that have relatively few component temperatures, this task becomes more difficult as surface complexity and the variety of materials present increases. To overcome this difficulty, we reduce the number of components in (1) to represent major surface orientations and use temperature frequency distributions to represent the actual variation of temperature due to microscale variations in surface properties.

As defined, T_c is not directly observable, although it may be possible to approximate it using hemispherical or wide FOV estimates of upwelling longwave radiation. These may provide a useful approximation because they reduce the directionality of the measurement and integrate both horizontal and vertical surfaces of all orientations. However, view factors for individual surfaces will be biased toward horizontal surfaces and those surfaces most directly beneath the sensor.

3. Study areas

The observational program was carried out using three primary study areas within the city of Vancouver, British Columbia, Canada. The sites selected included a light industrial (LI) area comprised of one- and two-story warehouses with flat roofs and workshops; a downtown office/commercial zone (D) with massive, tall buildings; and a suburban residential (R) neighbourhood composed of one- and two-story single family dwellings (Fig. 3).

In the R study area, vegetation cover (gardens, street trees, and parks) is extensive. Most streets have regularly spaced trees bordering the roadway. Although less frequent, trees are randomly distributed in backyards and alleys. Both the suburban and downtown sites were almost devoid of vegetative cover. A descriptive summary of the sites is given in Table 2.

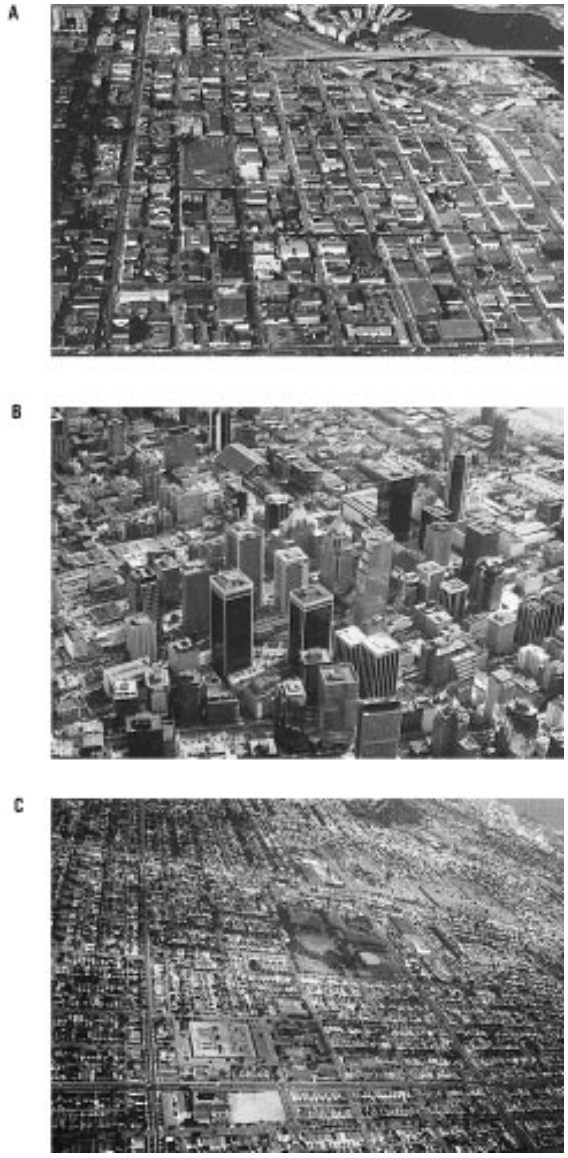

FIG. 3. Study areas in Vancouver, British Columbia, Canada. (a) Light industrial, (b) downtown, and (c) residential.

4. Methods

a. Estimating the complete surface area

1) BUILDINGS

The three-dimensional area of buildings A_b, made up of roof area A_r and wall area A_w (Fig. 2), is calculated using the digitized outlines of buildings taken from high-resolution (1:2500) aerial photography. Large rooftop structural elements such as elevator shaft housings are included, but structural details with length dimensions less than one-half the shortest building facet are omitted. Roofs may be planar or consist of two or four angled surfaces.

Building heights in the LI area were estimated in stories (to the nearest 0.5) with a story assigned as 3.7 m (12 ft). In area D, building heights (in stories) were obtained from Vancouver Planning Department (1984) maps. Building heights along the traverse route were updated from observations made using an Abney level. An eight-block subarea of the R study area was chosen for detailed analysis. Here, 271 houses (an average of 34 per block) and 139 garages (approximately 17 per block) were digitized. The height [in stories, to the nearest 0.25, using 3.05 m (10 ft) per story], roof type (flat, gabled, four-sided), and roof pitch were estimated for each building. Vertical facet surface area calculations for buildings with gabled roofs include the gables (triangular wall area above the level of the eaves on the end walls).

The area A of a polygon represented by a series of x_i, y_i points ($i = 1, N$) can be determined from Stoke's theorem as

$$A = \frac{1}{2}\left(\sum_{i=1}^{N-1} x_i y_{i+1} - y_i x_{i+1}\right) + x_N y_1 - x_1 y_N, \quad (2)$$

where the x, y values are the digitized points for each building or surface object. Vertical facet areas are obtained by calculating the length of a vector (side of the polygon) and multiplying this by the assigned height of the building.

Where adjacent buildings share a common wall, common vectors are identified. If the heights of the buildings differ, the area of the exposed wall is calculated. Wall

TABLE 2. Study site description. Bracketed designations for the sites are used in the text.

Site	Description[a]	Building heights	Street[b] pattern	Area (km^2)	Subarea[c] ($m^2 \times 10^3$)	No. of buildings
Downtown (D)	Office and commercial towers (C1)	6–20 stories	NE–SW NW–SE	0.56	453	274
Residential (R)	Single-family dwellings (R2)	1–2 stories	N–S E–W	1.0	170	409
Light industrial (LI)	Rectangular, closely spaced buildings (I2)	1–3 stories	E–W N–S	0.65	618	733

[a] Auer (1978) land-use category in brackets.
[b] Street pattern refers to the primary orientation of streets and cross streets. The direction of the long axis of the block is listed first.
[c] Subarea refers to the portion of the study area in which complete surface area calculations were made.

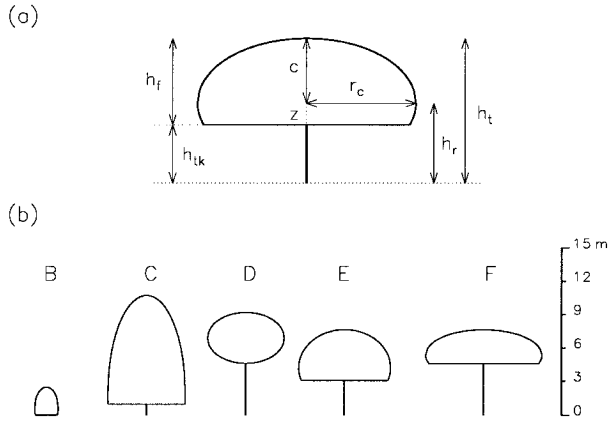

FIG. 4. (a) Definition of tree structural measures. (b) Modeled shapes for the tree types in the study area: B: bushes/shrubs, C: coniferous, D: deciduous, E: evergreen (nonconiferous), F: flowering (mainly cherry).

orientation is derived from the sign of (2) in combination with the slope (determined from the coordinates of the points relative to a reference point) of the line representing the wall segment.

2) TREES

Trees (in the R area only) were categorized into five types, based upon geometric form and relative abundance: B: bushes, C: evergreen (coniferous), D: broad leaved (deciduous), E: evergreen (nonconiferous), and F: flowering deciduous.

For surface area calculations, trees have been represented by the following simple shapes: cones (coniferous) (Li and Strahler 1985), spheres or cylinders (deciduous) (Jupp et al. 1986; Goel 1988) or, more generally, by ellipsoids (Campbell and Norman 1989). A wide variety of tree forms can be represented by ellipse parameters if the possibility of truncated ellipses is included (Charles-Edwards and Thornley 1973; Goel 1988).

Ellipsoids were used to represent the tree types present in the residential study area. Tree height h_r, maximum crown radius r_c, and height to the base of the foliage (equivalent to trunk height h_{tk}) were estimated from ground surveys for all trees in the study subarea. The position of the ellipse centroid (height of maximum crown radius h_r) was estimated as a fraction F_{hf} of the total foliage height h_f where h_f is the difference between h_i and h_{tk}. Here, F_{hf} was estimated to be 0.25, 0.1, 0.5, 0.25, and 0.1 for types B,C,D,E, and F, respectively.

Tree structural parameters are graphically portrayed in Fig. 4a. The ellipse semi-axes are represented by c and r_c (equivalent to a). When $z = c$, the tree canopy is represented by a complete ellipse; when $z < c$, the ellipse is truncated. Calculated shapes for select examples of each tree type in area R are presented in Fig. 4b. Crown radius is assumed to be symmetrical (i.e., circular) in the x and y planes; the tree shapes are elliptical in the x, z plane only, so the resulting shapes are most precisely described as prolate and oblate spheroids. Estimates of total tree surface areas calculated using the ellipsoidal representations versus those based on cones, cylinders, and spheres (assigned to representative tree types) agree to within 4%.

The representation of trees as simple geometric objects fails to account for gaps in the foliage, which reduce the projected surface area. The actual ''viewed'' or apparent surface area emitting outside the canopy in a particular direction is theoretically defined as the projection of the total canopy foliage onto a plane orthogonal to the direction of view. Lang and McMurtrie (1992) describe the theoretical basis for the commonly required case of foliage projected onto a horizontal plane below the canopy. The complete surface area of a tree canopy A_v may be defined as the area of foliage projected onto the bounding surface of the geometric shape representing the tree. This is the area of foliage that emits directly to the surroundings. Theoretical calculation of this value is complex.

As an approximation we define a ratio F_{gap} that is the reduction factor required to account for the gaps in the canopy foliage. The ratio F_{gap} allows the complete canopy area to be calculated from the simple geometric area, which in turn can be estimated from basic structural parameters. Calculation of F_{gap} is theoretically difficult and requires details of the canopy foliage density, orientation, and clumping. Values of F_{gap} obtained from the literature often refer to forest canopies rather than single trees and are generally based upon a cumulative projection of the leaf area index (LAI) onto a horizontal plane beneath the canopy. These values therefore do not account for the anticipated variations in F_{gap} for projections in the vertical plane. The F_{gap} estimates for model poplar stands based upon downward cumulative LAI (Chen et al. 1993) are in the range of 0.3–0.2 for a deciduous LAI of 4, which is the estimated maximum in the study area (Kramer and Kozlowski 1979; Grimmond 1988).

For this study it was considered acceptable to use crude approximations for F_{gap} based upon field observations. Tree types B–F were estimated to have F_{gap} values of 0.15, 0.2, 0.3, 0.2, and 0.45, respectively. If the structure of individual trees differed significantly from the average for their type, an estimated field value replaced the default value.

3) COMPLETE SURFACE AREA

The complete active surface area A_c of each study site is estimated by adding the (three-dimensional) areas of vegetation A_v and buildings A_b to that of the exposed ground area A_o:

$$A_c = A_v + A_b + A_o. \quad (3)$$

The area of exposed horizontal ground surfaces (A_o; grass, roads, etc.) is determined as a residual from

$$A_o = A_p - [A_{\text{pr}} + A_{\text{pv}(h_{\text{tk}}=0)}], \quad (4)$$

in which A_p is the total plan area (calculated from a topographic map), A_{pr} is the plan area of roofs (assumed equivalent to buildings), and $A_{\text{pv}(h_{\text{tk}}=0)}$ is the plan area of vegetation elements for which the canopy intersects the ground (most common for bushes but also some coniferous trees). The exposed ground area A_o includes horizontal surfaces below tree canopies where $h_t > 0$ (Fig. 2).

b. Infrared thermometry

1) Vehicle traverses of vertical facet surface temperature

An array of infrared thermometers (Everest Interscience Model 4000A, hereafter referred to as EIRT) was mounted on a truck to sample the temperatures of vertical surfaces (primarily building walls). The EIRT has a 15° FOV. The sensors were mounted in pairs facing outward from the vehicle. Traverses in the LI and R areas, where building heights were low, were conducted with one pair of sensors facing outward from each side of the vehicle. One sensor of each pair was level, while the other was mounted at a 10° elevation angle to sample the upper portions of the buildings. This configuration allows both sides of the street to be sampled with one traverse. In the D area, all sensors were oriented to face in the same direction with elevation angles of 0°, 15°, 30°, and 45° in order to better sample the temperatures of the tall buildings.

In both configurations, a single, downward-facing EIRT was used to obtain the road surface temperature, and air temperature was monitored using shaded and aspirated fine-wire thermocouples. Spatial sampling was conducted along a traverse route that covered all streets and alleyways (within a select area) in the LI and R study areas. Traffic considerations confined the traverse route in area D to streets only. A difficulty with the sampling methodology is that there is no record of what the sensors see when a sample is registered. Because of the unevenness of building heights and their spacing, samples are made up of not only building walls but also mixed FOV scenes composed of building and sky components or, in some cases, sky alone. This presents difficulties in the interpretation of the data, particularly for sunlit facets that have a wide range of surface temperatures. In this study the spectrum of temperatures recorded during a traverse is truncated, so that the low temperature end, characteristic of mixed building and sky or sky scenes, is removed.

2) Airborne infrared thermography

An AGEMA 880 LWB thermal scanner operating in the 8–14-μm waveband was mounted in a helicopter and used to obtain thermal images over each of the study areas from nadir and 45° off-nadir sensor angles. The imagery was corrected for atmospheric effects using the LOWTRAN-7 atmospheric radiation program (Kneizys et al. 1988) in conjunction with meteorological observations from airsondes (AIR Inc.) launched adjacent to the site. No correction for the effects of surface emissivity was made. Roth et al. (1989) suggest spatial temperature errors of up to 1.5 K are possible due to variations in urban–rural surface emissivity for satellite-based studies. Temperature variations due to emissivity differences are expected to maximize at scales on the order of meters and to decrease as averaging occurs over larger ground resolution element. High-resolution thermal imagery requires emissivity information beyond the scope of this project, and use of an overall urban emissivity (e.g., Arnfield 1982) does not necessarily imply complete correction of apparent surface temperatures on a pixel-by-pixel basis.

Flights were conducted at times when surface temperature contrasts between opposing street canyon facets were large. These times were selected to determine the presence and magnitude of effective anisotropy (directional variations in apparent surface temperature) over the study area (Voogt 1995). For the north–south and east–west street orientations of the LI and R areas, this led to flights in the morning, slightly after solar noon, and in the late afternoon. In the D study area, where the street pattern is aligned northwest-southeast and northeast-southwest, flights were conducted in the late morning and midafternoon.

c. Estimating the complete surface temperature

The complete surface temperature, defined by (1), requires specification of surface emittance for each of the area components included in the summation. If areas are defined on the basis of having different temperatures, the procedure becomes difficult to implement in urban areas where there is a wide variety of surface types to consider (e.g., Quattrochi and Ridd 1994). Rather than defining myriad surface types and prescribing their representative temperatures, an alternate approach was devised. It uses frequency distributions of apparent temperature either from the airborne AGEMA imagery or in combination with the vehicle traverse EIRT data.

1) Combination of nadir airborne and traverse temperature distributions

One method to estimate T_c is to combine the apparent surface temperature distributions of horizontal surfaces from airborne nadir scanner imagery with those of vertical facets obtained from the vehicle traverse (Fig. 5). This horizontal–vertical combination circumvents the need to subdivide the horizontal surface into component fractional areas and estimate mean temperatures or temperature distributions for each. The observed nadir tem-

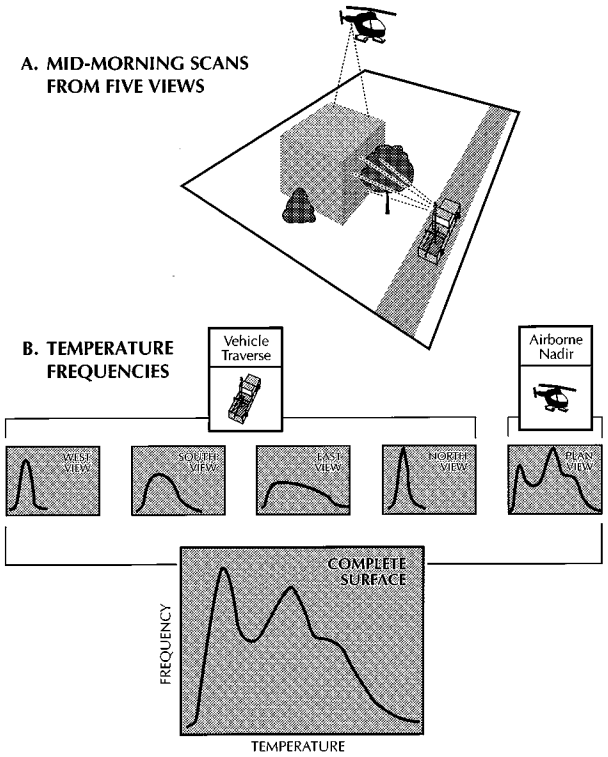

FIG. 5. Conceptual representation of the procedure to calculate the complete surface temperature distribution for an urban area by combining airborne nadir and ground-based vertical facet temperature distributions.

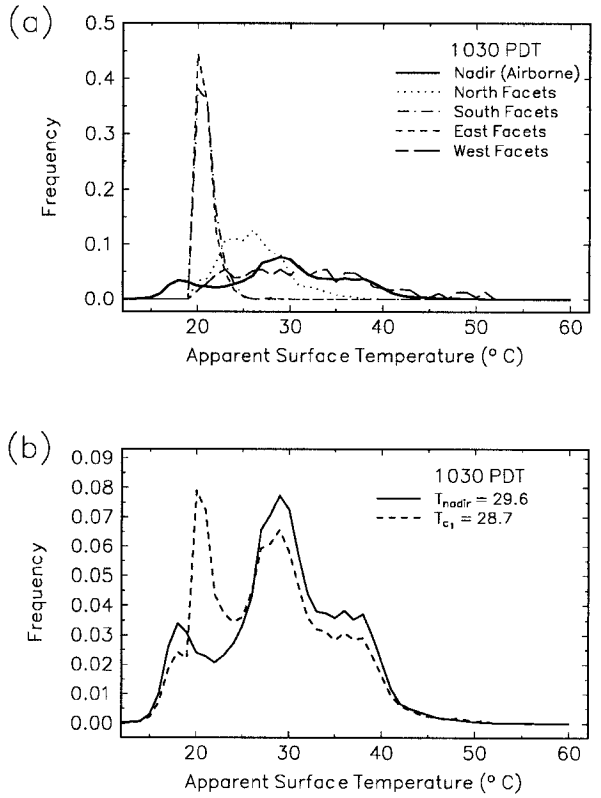

FIG. 6. (a) Frequency distributions of surface temperature for components in the Industrial area, 1030 PDT 15 August 1992. Vertical facet distributions are from the vehicle traverse. (b) Composite temperature distribution of the LI study area from the airborne nadir imagery and the complete surface temperature composited from (a).

perature distribution is assumed to represent the various components in their correct proportions. The component frequency distributions (nadir and four vertical) are combined with weights according to their fraction of the complete surface area. In the residential area where trees obscure some portion of the horizontal surface, an additional weighting for the obscured horizontal surface is included. The temperature for this surface was obtained from ground observations made by personnel equipped with handheld infrared radiation thermometer (IRT).

Figure 6a illustrates the component temperature distributions from the airborne and vehicle observations from a morning flight over the LI area. These are combined as illustrated in Fig. 5 to create the complete surface temperature distribution presented in Fig. 6b. The mean emittance of the complete distribution is estimated using (1), where f_i are the frequencies for each emittance class and L_i is the emittance for the class. Then T_c is obtained by inversion of the Stefan–Boltzmann law. A disadvantage of this approach is the need to truncate or otherwise modify the distribution of surface temperatures obtained from the vehicle traverse to remove mixed building and sky values. This procedure has the advantage of including most observations that fully view wall surfaces, but it also retains some observations of mixed sky and warm wall surfaces, which yield a combined temperature greater than the truncation temperature. The resulting distribution slightly underestimates areas of high surface temperature. A second difficulty is that the method assumes that the distribution of vertical facet temperatures is representative of all vertical surfaces. In practice the traverse method restricts observation to facets that may be viewed from positions along the route and are within the range of elevation angles of the EIRT. Facets orthogonal to the street are not sampled except on the ends of the block. Unfortunately, close interbuilding spacing means that end facets have greater exposure to direct solar radiation than for similarly oriented facets within the block. Calculations for the R area indicate 57%–80% of the area of interbuilding walls are shaded during the times of the morning and late afternoon flights, depending upon the building height and spacing. During the early afternoon flight, 35%–55% are shaded.

2) COMBINATION OF NADIR AND OFF-NADIR AIRBORNE

An alternative to the use of the vehicle traverse data is to use vertical facet surface temperature distributions extracted from the off-nadir airborne scanner imagery.

TABLE 3. Major surface component areas for each study area: LI: Light Industrial, D: Downtown, and R: Residential. All areas have units of $m^2 \times 10^3$.

Area	Symbol	Area (LI)	% of A_c	Area (D)	% of A_c	Area (R)	% of A_c
Plan (2D)	A_p	618	71	453	46	170	56
Ground level	A_o	380	44	287	29	121	40
Roof	A_r	237	27	167	17	53	17
Wall (N or NE)	$A_{w(N, NE)}$	69	8	138	14	23	8
Wall (S or SE)	$A_{w(S, SE)}$	70	8	137	14	23	8
Wall (E or NW)	$A_{w(E, NW)}$	55	6	134	13	17	6
Wall (W or NW)	$A_{w(W, NW)}$	54	6	133	13	17	6
Wall (misc.)	$A_{w(M)}$	9	1				
Vegetation	A_v					52	17
Complete	A_c	875		995		306	
Total Active (3D/2D)	A_c/A_p	1.4		2.2		1.8	

These overcome some of the difficulties with the traverse vehicle data but have their own limitations. Results from the extracted data depend on the completeness with which component surface areas are sampled because temperature patterns are the sole means of defining the spatial dimensions of the facets. In the R and D areas, where interbuilding spacing is small, it may be difficult to obtain the temperature of facets due to the small area seen at the off-nadir angle.

Tree canopy temperatures are estimated for each view direction in the R area. The difference in area between A_v and A_{pv} was divided equally among the four view directions; the vertical plan area of vegetation is included in the nadir weighting. A weighting for the obscured horizontal ground area is also included.

5. Results

a. Complete surface areas of the study sites

Component surface areas, calculated from the database of surface structure, for each of the study areas are presented in Table 3, and frequency distributions of building height are shown in Fig. 7a. Heights are distributed approximately normally in the LI and R areas, with only a few instances of tall (>4 stories) buildings. In area D, the distribution is strongly asymmetric with greatest frequencies in classes centered between 5 and 15 m and a long tail of frequencies extending toward higher building heights.

In the LI area combined wall areas constitute 28% of A_c and horizontal surfaces (including rooftops) make up the remaining 71%. Greater areas of north- and south-facing facets are exposed compared to east- and west-facing because many of the buildings along the blocks share common east and west walls and therefore have no east or west exposure (Fig. 3a). In area D, vertical facets combine to form 54% of A_c, a value greater than the fraction of horizontal surfaces (46%) and much greater than the horizontal roof area (17%, Table 3). The percentage wall area in area R is similar to that of the LI area; this result is likely due to the high incidence of common building walls in the LI area which reduces the relative wall area.

Surface area calculations for the R site include the effect of roof pitch so that both plan roof area and actual roof area are available. The mean roof pitch in area R is approximately 20°, although the distribution is skewed, with substantial numbers of both houses and garages observed to have higher roof pitch angles. Roof types are fairly equally split among gabled and four-sided types; only a minor proportion have flat roofs.

As a measure of building density the ratio of roof to plan area yields values of 38%, 37%, and 31% for areas LI, D, and R, respectively. The active area ratio A_c:A_p, is a measure of the increase in effective surface area in contact with the atmosphere due to the three-dimensionality of the urban interface. In the study areas the increase is about 40% in LI, 80% in R, and about 120% in D (Table 3). Trees are a major contributor to the large A_c:A_p value calculated for the R area.

Results of the survey of tree structural parameters are presented in Table 4. Deciduous trees are the most frequently occurring type, accounting for 59% of the total. The overall mean tree height (not including type B) is 7.7 m. This is only approximately 50% of the height adopted by Schmid (1988). The difference between the two estimates is attributed to the small spatial domain in the current study and the abundance of relatively small street trees. A two-dimensional projection of the canopy area, less the two-dimensional area of trees where foliage intersects the ground, yields the obscured horizontal surface area (12547 m^2, 4.1% of A_c).

b. Viewed and nonviewed surfaces

A summary of surface areas broken down into those surfaces generally seen or viewed by remote sensors (i.e., horizontal, unobstructed surfaces) and those most often unseen or undersampled (e.g., building walls or obstructed horizontal surfaces) is given in Table 5. Also included are results from a typical high-rise housing estate in Singapore (Nichol 1996). The results highlight

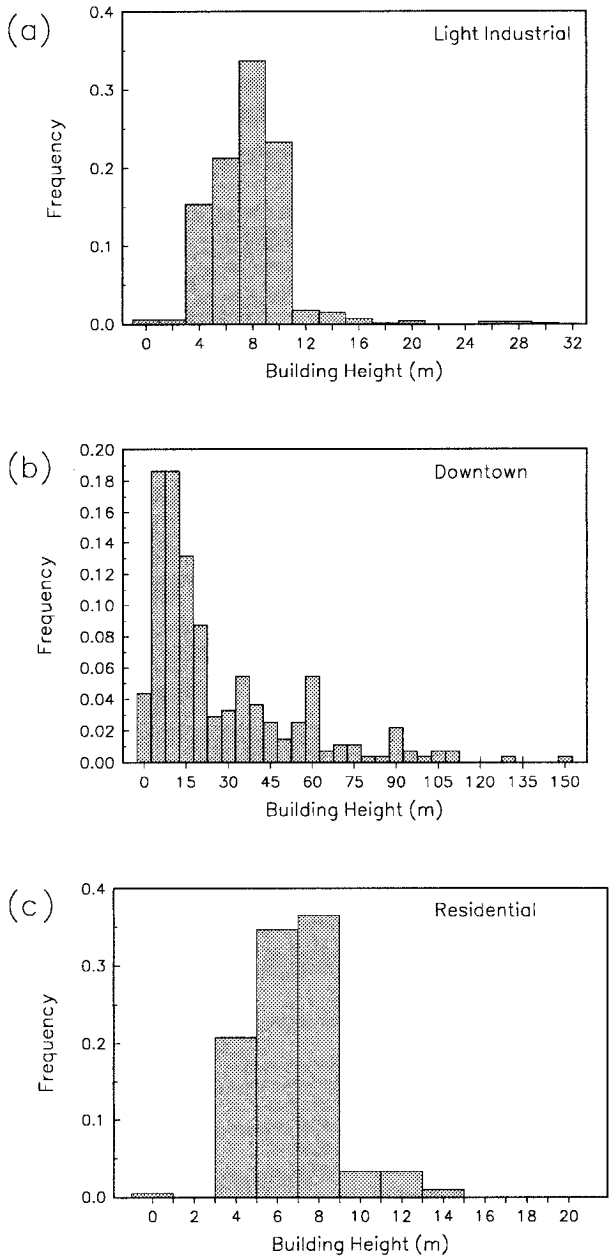

FIG. 7. Frequency distribution of building heights in (a) LI, (b) D, and (c) R study areas.

TABLE 5. Proportions of ''seen'' and ''unseen'' areas. Singapore results from Nichol (1996).

Area	Vancouver D	Vancouver LI	Vancouver R	Singapore
Seen (2D)				
Ground	0.63	0.62	0.64	0.77
Roofs	0.37	0.38	0.28*	0.17
Tree canopies			0.08	0.16
Unseen				
Walls	1.20	0.40	0.47	0.54
''Below''-tree canopies			0.30**	0.16
Total active surface	2.2	1.4	1.8	1.7

* Plan projected roof area, which is slightly less than the total roof area and accounts for the missing 0.03 required for the sum to equal 1.8.

** Calculated as ground area below tree canopy plus the difference between 3D tree canopy area and the plan projected tree canopy area.

the importance of building walls and obscured areas as a component of the complete urban surface.

The Vancouver sites all show similar values for the proportion of open ground (roads, grassed areas, etc.). Roofed areas are largest in the LI and D areas of Vancouver. Roof pitch in residential areas increases the effective roof area relative to the building plan area. Tree canopies are not included in the analysis of the D and LI areas, but this should not be a significant omission. The value for the R area is based upon the tree structural information gathered by field surveys rather than areal estimates from aerial photographs.

Wall areas make up the most significant proportion of unseen areas with the fraction highest in area D. Wall areas for the LI and R areas are similar; the LI area is probably reduced somewhat because of the large number of buildings that share adjoining walls. Despite the smaller plan vegetated area, the ''below''-tree canopy area for site R is larger than Singapore because this area includes a portion of the three-dimensional vegetated area (see Table 5).

c. Complete surface temperatures of the study sites

1) COMPARISONS OF T_{c_1} AND T_{c_2}

The mean vertical facet temperature distributions obtained from the airborne and vehicle platforms for all flights over the LI and D study areas are compared in Fig. 8. Comparison with the R area is not possible be-

TABLE 4. Statistical summary of the dimensions of tree structural parameters from field surveys. Units are in meters.

Tree type	Code	n	h_t Mean	h_t σ	h_t Med.	r_c Mean	r_c σ	r_c Med.	h_{tk} Mean	h_{tk} σ	h_{tk} Med.
Bush	B	81	2.4	1.2	2.4	1.1	0.4	0.9	0.1	0.3	0
Coniferous	C	78	8.6	4.1	9.1	3.1	2.2	2.4	1.8	1.7	1.4
Deciduous	D	289	7.7	3.2	7.6	3.4	1.6	3.1	3.2	1.8	3.1
Flowering deciduous	F	43	6.2	1.8	6.1	3.0	1.3	3.0	2.7	1.5	2.1

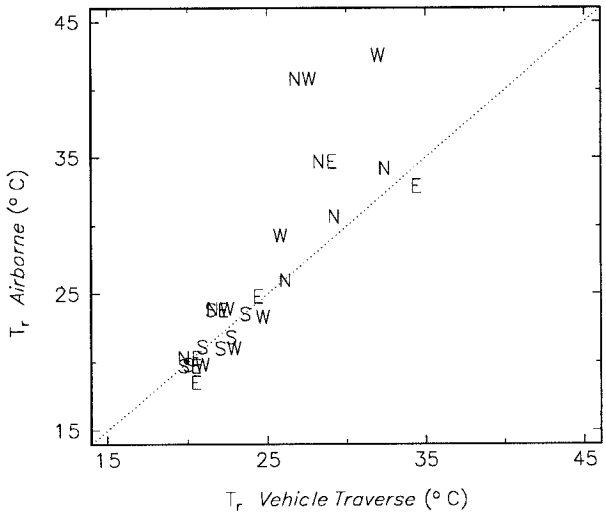

FIG. 8. Comparison of apparent wall surface temperatures for the D and LI areas obtained from vehicle traverses and the airborne thermal scanner. Symbol letters refer to facet orientation.

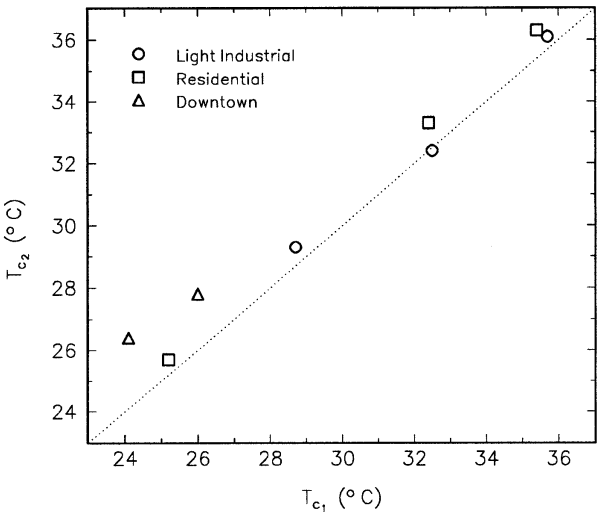

FIG. 9. Comparison of complete surface temperatures calculated using combined airborne nadir and vehicle traverse data (T_{c_1}) vs that using airborne nadir and off-nadir data (T_{c_2}).

cause the vehicle traverse includes building facet and vegetation temperatures, whereas these components were extracted separately in the remotely sensed imagery. Agreement is generally good when facet temperatures are cool (i.e., they are mostly shaded). At higher temperatures there are significant biases, particularly in the D area. This bias is attributed to differences in viewing location between the two observation platforms. From the perspective of the airborne scanner, warm bias may be attributed to one or more of the following: A preferential view of the top (fully irradiated) portion of walls, inability to view below the level of any awnings (which shade the lowest portions of the building walls), obscuration of the lower wall when canyon geometry (i.e., H/W) is large, and specular reflection of radiation from warm street and canyon surfaces by facets with low emissivity. Vehicle traverse results have a cool bias using a similar reasoning.

Differences in the LI area may be related to sampling biases induced by the particular building geometry. The vehicle traverse and airborne scanner sample north and south facets equally well since the street pattern allows full access by the traverse vehicle. However, many east and west walls along a block cannot be viewed from the traverse vehicle since they do not directly face onto a street. Further, these facets tend to be warmer because they have greater solar access earlier in the morning and evening than do the end-of-canyon walls, which are more subject to shading by buildings on the opposite side of the street. A similar vehicle sampling bias exists for the R area; however, here the very narrow interbuilding spacing and pixel smearing also prevents good sampling of the wall surfaces using the image extraction technique.

The biases in facet temperature are reflected in the comparison of T_{c_1} and T_{c_2} for each site (Fig. 9). The differences between estimates are largest in area D (up to 2°C) where the sampling biases are greatest.

In the R area, T_{c_1} uses combined 0° and 10° EIRT temperature distributions from the traverse vehicle, and it is assumed that an adequate sampling of both the house and tree temperatures is obtained. Truncation of the traverse distribution was specified using a graphic analysis of the traverse and extracted temperature distributions, and looking for evidence of the tree canopy signal in the traverse (especially 10° EIRT) distribution. This was related to a local minimum in the frequency distribution.

Estimates of T_{c_2} combine extracted temperature distributions for vertical facets and tree canopies. Off-nadir tree canopy temperature distributions show variations in the mean of approximately 3°C between the most directly irradiated direction and the most shaded for each flight over the R area. This is similar to the magnitude observed by Balick et al. (1987), McGuire et al. (1989), and Sun and Mahrt (1995).

2) COMPARISON OF COMPLETE AND REMOTELY SENSED TEMPERATURES

Comparison of complete temperature estimates with the airborne nadir and off-nadir mean apparent temperatures (denoted generally as T_r, or specifically by T_{nadir} or $T_{\text{off-nadir}}$) allows us to determine the degree to which remotely sensed observations are biased. In general, the most apparent difference between the complete and nadir temperature distributions is the enhancement of low temperature frequencies. This occurs because, except for the most directly irradiated facet, all vertical surfaces have temperature distributions that are cooler than those in the horizontal. Temporally, the difference between the nadir and vertical distributions is strongest

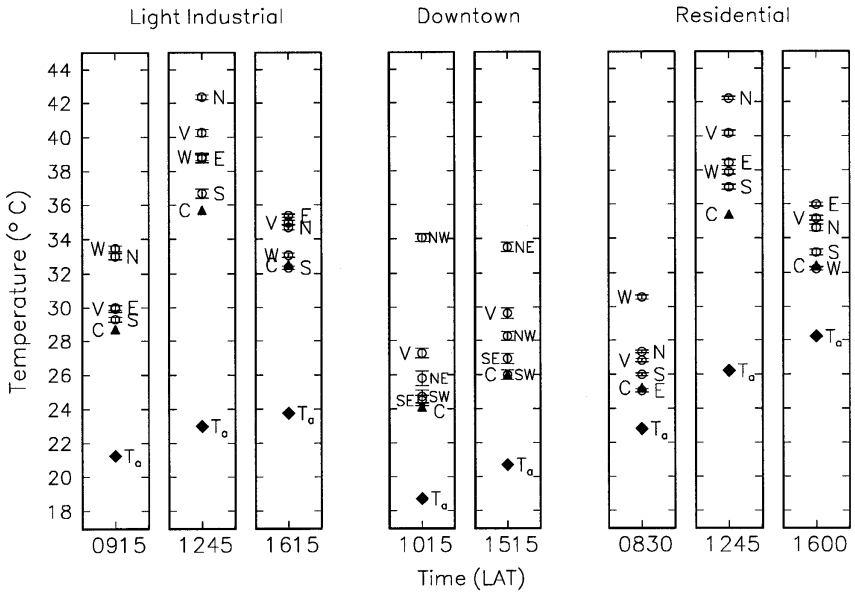

FIG. 10. Comparison of complete apparent surface temperatures T_{c_1}, (solid triangles labeled C) with mean image apparent surface temperatures labeled by view direction (V: nadir), and traverse air temperatures (T_{at}, denoted by solid diamonds) for all study areas and flight times.

near solar noon when, because of the relatively small zenith angle, even the most directly irradiated facet has a distribution significantly cooler than the horizontal. At times earlier and later in the day, the most directly irradiated wall has a frequency distribution only slightly cooler than that of the horizontal, so T_c estimates are closer to T_{nadir}.

Following sunset and with conditions favoring strong radiational cooling, it is possible that T_c may become warmer than T_{nadir} or $T_{\text{off-nadir}}$. Under these conditions, the sky view factor (as controlled by surface geometry) and surface thermal properties exert a strong control on the resulting surface temperature pattern: roofs, treetops, and horizontal open areas, especially those with low thermal admittance, become cool, while the lower portions of the building walls and nearby horizontal surfaces remain warm. Remotely observed apparent surface temperatures may therefore be cooler than the complete surface if the view is biased toward horizontal, unobstructed surfaces. For off-nadir viewing geometries, results may be sensitive to the particular surface geometric configuration. No nighttime observations are available from this study to test these hypotheses.

Complete, nadir, and off-nadir temperatures in each view direction for each of the study areas and all flight times are presented in Fig. 10, where T_c is represented by T_{c_1}. All observations at nadir, and most of those at off-nadir, are warmer than T_c. The single observations that most closely match T_c are those off-nadir observations with view angles in the direction of the most shaded facet (north or northeast walls). On all occasions, T_{air} is considerably (3°–12°C) lower than T_c.

It is evident from Fig. 10 that urban surfaces are characterized by strong directional variations of apparent surface temperature (anisotropy), especially between surfaces viewed with the sensor in an up-sun, versus a down-sun, direction. The variations between complete and remotely observed temperatures can be large when the remote sensor views the surface in the direction of the most directly irradiated vertical surface; maximum observed differences for the LI, R, and D areas were 6°, 10°, and 7°C, respectively. These differences are large in comparison to other influences upon remotely observed surface temperature. Our estimate of the effect of emissivity is 1.5°–2.5°, which is an upward adjustment of the 1.5° estimate by Roth et al. (1989) due to anticipated larger variations in surface emissivity at smaller observational scales. Further errors due to the presence of specularly emitting surfaces in the thermal infrared are possible, especially in downtown environments. These would generate nonisotropic radiance distributions, but detailed analysis of their effect has yet to be undertaken. Variations due to atmospheric absorption and emission along the path length viewed by the sensor are on the order of 4°–7° (assuming midlatitude summer conditions) as determined from observations and model simulations (LOWTRAN-7). Spatial variations in atmospheric properties over large cities have been estimated to contribute infrared signals equivalent to about 1 K (Carlson 1986).

The influence of view direction on the relationship between T_c and remotely measured mean apparent surface temperature for each of the study areas is given in Fig. 11. So that results from all three study areas may be viewed simultaneously, the flight data over the D study area have been combined by assigning facets as

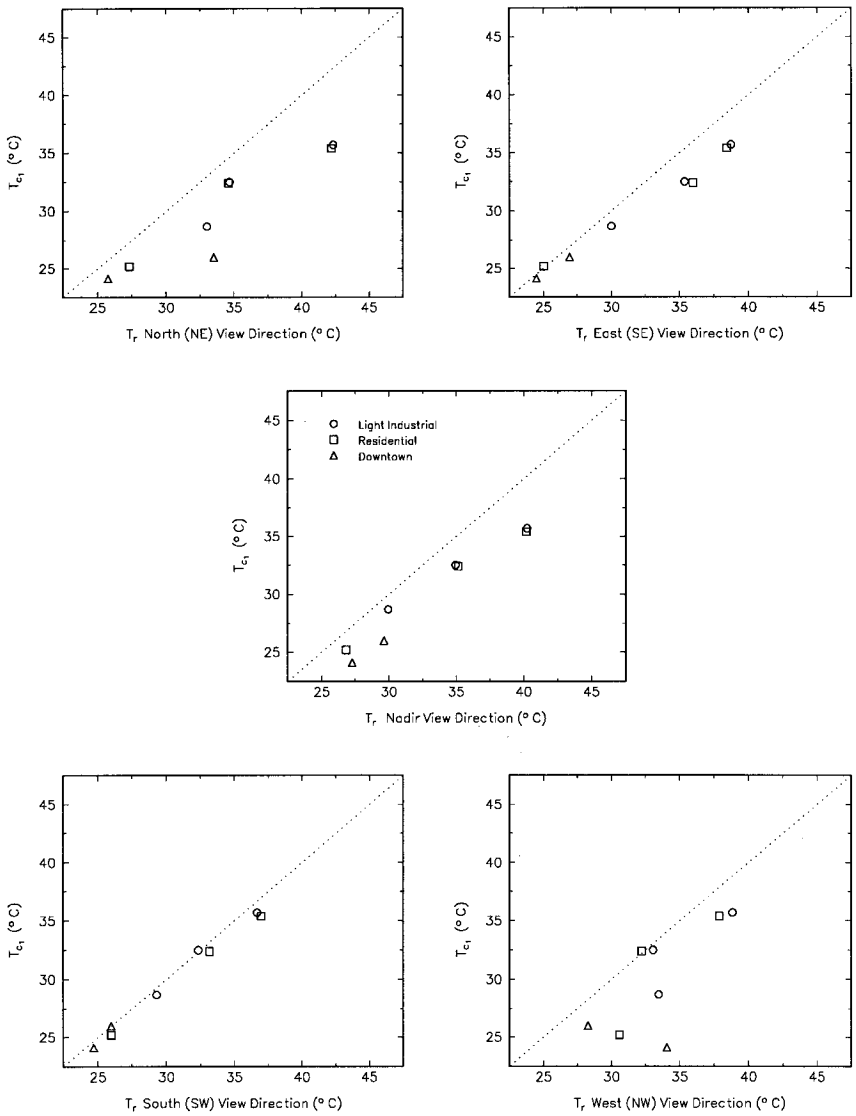

FIG. 11. Comparison of complete surface temperature with mean apparent temperature for each view direction. Data for all flights conducted over each study area are plotted. The convention for plotting data from area D northeast is congruent to north, southeast is congruent to east, northwest is congruent to west, and southwest is congruent to south.

northeast is congruent to north, southeast is congruent to east, northwest is congruent to west, and southwest is congruent to south. The relationship between T_{c_1} and T_r from south and east view directions shows remarkable linearity despite variations in time, surface structure, and temperature. In particular, the south view direction (which is most shaded) yields almost a 1:1 relationship and most observations agree within 1°C. The exceptions are LI and R shortly after solar noon, when the difference is about 2°C. This suggests that there is value in using the remotely sensed mean temperature in the direction of the most shaded vertical facets to directly estimate T_c.

From a predictive view point, it may be preferable to consider the relation between T_c and nadir observations, since most available remote sensors operate in this configuration. Using T_{nadir}, $T_{\text{off-nadir}}$, and the total active area A_c: A_p of each site as independent variables, linear regressions were performed on the results of Fig. 11. Results are presented in Table 6. When only one independent variable is used, $T_{\text{off-nadir}}$ in the most shaded direction performs slightly better than does T_{nadir}. The addition of A_c:A_p was found to be a statistically significant independent variable ($\alpha = 0.99$) and slightly improves the model statistics over those obtained from T_{nadir} alone.

The generality of the predictive relations is limited by the small sample size, limited temporal domain, view angle restrictions, and differences in building orientation of the current study. In practice, there is also the fact that T_c is most different from T_r for a single view

TABLE 6. Results of linear regression analysis for prediction of T_{c1} from Model A: T_{nadir}, Model B: $T_{off\text{-}nadir}$ (most shaded direction), and Model C: T_{nadir}, (A_c:A_p). Model performance statistics [rmse measures and d, the index of agreement (Willmott 1981)] are calculated from modeled T_c vs observed T_c.

Regression parameter	Model A	Model B	Model C
Constant	2.3581	0.585	9.990
Coefficient 1	0.8370	0.957	0.755
Coefficient 2			−2.8039
r^2	0.96	0.99	0.99
Total sum of squares	149.2	149.2	149.2
Resid. sum of squares	5.91	1.49	1.47
F	146	596	251
rmse	0.860	0.431	0.429
rmse (systematic)	0.171	0.043	0.043
rmse (unsystematic)	0.843	0.429	0.427
d (index of agreement)	0.998	0.989	0.998

direction shortly after solar noon (Fig. 10). This is relevant given that many remote sensing missions are flown near midday in order to capture the spatial distribution of surface temperature at the time of maximum surface temperature.

6. Application of complete surface temperatures

a. Complete surface and air temperature relations

Remote measurements of apparent surface temperature are often compared with surface-layer air temperature measurements (Dousset 1989; Henry et al. 1989; Stoll and Brazel 1992; Gallo et al. 1993; Lee 1993; Nichol 1996) with the goal of generating estimates of air temperature from thermal imagery. Results vary for the reasons discussed by Roth et al. (1989), namely, remote sensors incorporate a biased view of rough surfaces, air and surface temperatures have a complex coupling through flux divergence in the lowest layers of the atmosphere, and there are mismatches in the scales of observation used for remote and in situ measurements.

Estimation of complete surface temperatures addresses the problem of observational bias in the remote thermal measurements. The results here indicate that large differences exist between daytime apparent surface and air temperatures when compared at the land-use scale (Fig. 12a). Both traverse (canopy level) air temperatures and, where available, fixed tower measurements several meters above mean canopy height are plotted. Data from the LI and R sites exhibit similar diurnal trends (nonlinear) in the pattern of T_{air} versus T_r (nadir) or T_c. The use of T_{air} measured just above the canopy layer yields a slight reduction in the differences between the LI and R site. No such observations were available over the D study area.

The use of T_c in place of T_{nadir} only slightly enhances the predictive capabilities for estimating T_{air} (Fig. 12b). We conclude there is little utility in using simple regression techniques to predict T_{air} from remotely

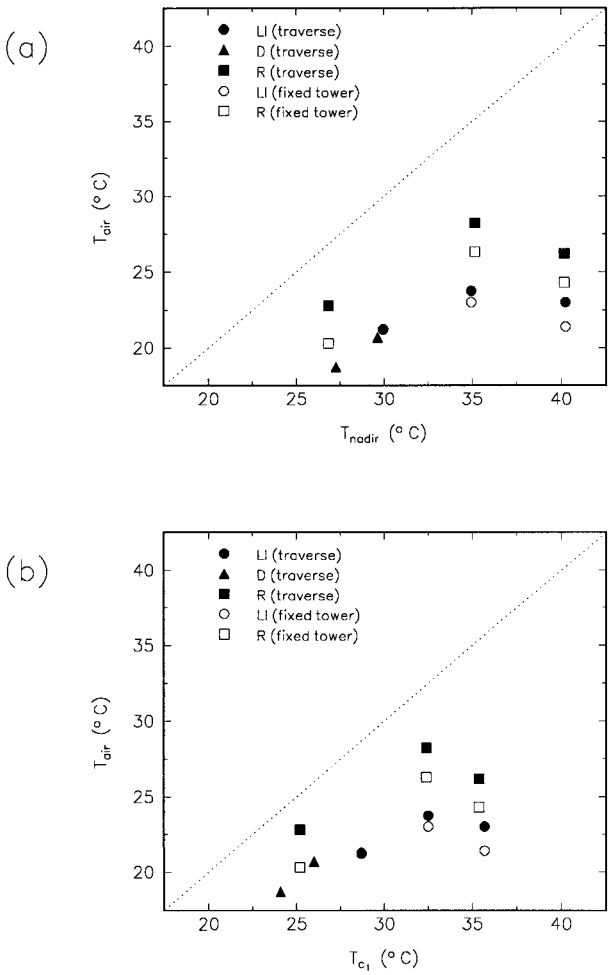

FIG. 12. Comparison of (a) air and nadir apparent surface temperatures and (b) air and complete surface temperatures.

sensed surface temperature. The physical linkage between the surface and the air is far too complex, especially in urban areas, to be amenable to such analysis (see also Stoll and Brazel 1992).

b. Surface temperatures and the surface energy balance

Much interest has been generated in the use of remotely sensed variables to predict the surface energy balance and the partition of net radiation into sensible, latent, and conductive heat components. Remotely measured surface temperature is used in formulations to estimate net radiation and sensible heat flux (e.g., Hall et al. 1992).

Net radiation can be determined using remote sensing to estimate each component of the radiation balance: downwelling shortwave and longwave radiation, surface albedo, and upwelling longwave radiation. If this is undertaken over cities, estimation of

the upward flux of longwave radiation should consider the effective anisotropy that exists in thermal emissions over these surfaces [see Fig. 10 and Voogt (1995)]. Complete surface temperatures could be useful as a means of accounting for the anisotropy of rough surfaces.

Calculation of the surface sensible heat flux Q_H can be accomplished using

$$Q_H = \frac{C_a(T_{\text{aero}} - T_{\text{air}})}{r_{ah}}, \tag{5}$$

where C_a is the volumetric heat capacity of air, r_{ah} is the resistance to heat transfer for the surface, T_{aero} is the surface aerodynamic temperature, and T_{air} is the air temperature just above the surface. The difficulty in applying remote sensing to the estimation of Q_H via (5) is that T_r, as measured by a remote sensor, is in general different from the aerodynamic temperature (Hall et al. 1992; Norman et al. 1995; Sun and Mahrt 1995). This occurs primarily due to the effects of surface emissivity and directional dependence on viewing angle [the effective anisotropy; Norman et al. (1995)]. Differences between T_r and T_{aero} are important because Q_H is sensitive to even small errors in the difference [$T_{\text{aero}} - T_{\text{air}}$; see, for example, Norman et al. (1995) and Kohsiek et al. (1993)]. Here, we calculate variations in Q_H for site R when T_r and T_c are used in place of T_{aero}. The calculations use the method of Kustas et al. (1989). The site has a roughness length of $z_0 = 0.52$ m and a zero-plane displacement length of 3.5 m (Steyn 1980); other input conditions were obtained from observations taken at the sunset tower, which is located in site R (Roth and Oke 1993) during the time of the remote sensing overflights. The parameter kB^{-1}, the added resistance of a surface to heat transfer (e.g., Garratt 1992; Brutsaert 1982), has been shown to have a reasonably constant value of 2.5 over a range of vegetative surfaces, including partial canopy covers, but bluff-rough surfaces are characterized by much higher values. Kohsiek et al. (1993) report $kB^{-1} = 3.68$ over a mixed short vegetation and stone surface, with the suggestion that a rock surface may have values on the order of 8–10. The urban residential area has a combination of solid and permeable roughness elements with a partial canopy cover, so kB^{-1} may be intermediate between the values for vegetation and bluff bodies. We performed calculations by setting kB^{-1} at constant values of 2.5, 5, and 10; using values for bluff-rough surfaces from Brutsaert (1982); and using the back-calculated kB^{-1} required to match the observed Q_H and r_{ah} for the site (S. Grimmond 1997, personal communication). The use of the bluff-body curve presented by Brutsaert (1982) yields kB^{-1} in the range of 22–27. Matching kB^{-1} to the tower observations of Q_H and r_{ah} (which solves for the required temperature gradient) yields $kB^{-1} \approx 3$.

The results show Q_H may vary from 12 to 85 W m^{-2} °C^{-1} for the observed range of T_r and T_c, depending upon the time of day, atmospheric conditions, and kB^{-1}. These values are of similar magnitude to those given by Norman et al. (1995). Differences in Q_H due to the method of calculation of T_c are generally 10%–20%. When T_{nadir} is used in place of T_c, differences are 15%–31% in the morning and rise to 15%–40% later in the day as the difference $T_{\text{nadir}} - T_c$ increases. Variations in calculated Q_H due to the use of off-nadir remotely measured temperatures often exceed 50% when comparing $T_{\text{off-nadir}}$ in the up- and down-sun directions and can be greater than 100% when comparing the most directly irradiated facet with T_c. In accordance with the close agreement between the temperature of the most shaded facet and T_c, differences in Q_H are minimized (generally less than 5%) for this temperature pair.

Comparison of $Q_{H(\text{obs})}$ and $Q_{H(\text{est})}$ using r_{ah} calculated from the tower site data suggests that the required temperature gradient for Eq. (5) is too large, particularly at midday. The use of T_c in place of T_r improves Q_H estimates; however, T_c remains warmer than the temperature required (T_{aero}) to satisfy $Q_{H(\text{est})} = Q_{H(\text{obs})}$. The required temperature is approximately 2°–2.5° cooler than T_c in the morning and late afternoon and 7° cooler in the early afternoon. It is possible that this difference may be due partly to an underestimation of the shaded portion of the complete surface estimate, which is less apparent in the morning and late afternoon when T_{nadir} incorporates more shaded surfaces than in the early afternoon. A more detailed comparison of the tower-mounted flux estimates for the LI and R sites and those derived using remotely sensed and complete surface temperatures is under way.

7. Conclusions

This work presents the first attempt to calculate a complete surface temperature that takes into account both the horizontal and vertical surfaces in urban areas and thus recognizes the thermal impact of the three-dimensionality of the system. Complete surface temperature estimates are shown to generally differ from remotely sensed estimates of urban surface temperature whether they view the city from nadir or off-nadir. These findings are true for the three land-use types studied. Off-nadir observations in the direction of the most shaded facet agree most closely with T_c and provide a useful first approximation to its estimation. The limited data available suggest this approximation is least valid at midday. During the daytime, complete surface temperatures are greater than air temperature by several degrees.

Currently, our findings serve primarily as a warning of the dangers of using remotely observed surface temperatures without regard to the geometric nature

of the surface being observed and the viewing conditions. We emphasize the need to match scales of observation with those of analysis and to recognize, for a given application, which surfaces and which physical variables are of importance (e.g., air, surface, or aerodynamic temperature). Work is under way to develop and assess methods to estimate T_c from remote temperature observations and to further consider the effect of scale. Further work requires looking at the usefulness of complete surface temperatures to the estimation of air temperature and energy balance fluxes over urban areas, and how significant the role of surface emissivity is in these matters.

Acknowledgments. Thanks are due to Drs. R. Spronken-Smith and S. Grimmond for assistance with the field observations. Drs. S. Grimmond and M. Roth provided helpful suggestions regarding the surface energy balance calculations. The AGEMA scanner was made available by the Ontario Laser and Lightwave Research Centre. P. Chalk assisted with the preparation of the figures. This work was supported by grants from the Natural Sciences and Engineering Research Council of Canada and the Atmospheric Environment Service of Environment Canada.

REFERENCES

Arnfield, A. J., 1982: An approach to the estimation of the surface radiative properties and radiation budgets of cities. *Phys. Geogr.*, **3,** 97–122.

Balick, L. K., B. A. Hutchison, J. A. Smith, and M. J. McGuire, 1987: Directional thermal infrared exitance distributions of a deciduous forest in summer. *IEEE Trans. Geosci. Remote Sens.*, **GE-25,** 410–412.

Boissard, P., G. Guyot, and R. D. Jackson, 1990: Factors affecting the radiative temperature of a vegetative canopy. *Applications of Remote Sensing in Agriculture*, M. D. Steven and J. A. Clark, Eds., Butterworths, 45–72.

Brutsaert, W., 1982: *Evaporation into the Atmosphere: Theory, History and Applications*. Reidel, 299 pp.

Campbell, G. S., and J. M. Norman, 1989: The description and measurement of plant canopy structure. *Plant Canopies: Their Growth, Form and Function*, G. Russell, B. Marshall, and P. G. Jarvis, Eds., Cambridge University Press, 1–19.

Carlson, T. N., 1986: Regional scale estimates of surface moisture availability and thermal inertia using remote thermal measurements. *Remote Sens. Rev.*, **1,** 197–247.

Charles-Edwards, D. A., and J. H. M. Thornley, 1973: Light interception by an isolated plant: A simple model. *Ann. Bot.*, **37,** 919–28.

Chen, S. G., I. Impens, R. Ceulemans, and F. Kockelbergh, 1993: Measurement of gap fraction of fractal generated canopies using digitalized image analysis. *Agric. Forest Meteor.*, **65,** 245–259.

Dousset, B., 1989: AVHRR-derived cloudiness and surface temperature patterns over the Los Angeles area and their relationships to land-use. *Proc. IGARSS-89*, Vancouver, BC, Canada, IEEE, 2132–2137.

Gallo, K. P., A. L. McNab, T. R. Karl, J. F. Brown, J. J. Hood, and J. D. Tarpley, 1993: The use of a vegetation index for assessment of the urban heat island effect. *Int. J. Remote Sens.*, **14,** 2223–2230.

Garratt, J. R., 1992: *The Atmospheric Boundary Layer*. Cambridge University Press, 316 pp.

Goel, N. S., 1988: Models of vegetation canopy reflectance and their use in estimation of biophysical parameters from reflectance data. *Remote Sens. Rev.*, **4,** 1–212.

Grimmond, C. S. B., 1988: An evaporation-interception model for urban areas. Ph.D. thesis, University of British Columbia, 206 pp. [Available from the University of British Columbia Library, Special Collections, 1956 Main Mall, Vancouver, BC V6T 1Z1, Canada.]

Hall, F. G., K. F. Huemmrich, S. J. Goetz, P. J. Sellers, and J. E. Nickeson, 1992: Satellite remote sensing of surface energy balance: Success, failures, and unresolved issues in FIFE. *J. Geophys. Res.*, **97** (D17), 19 061–19 089.

Heilman, J. L., W. E. Heilman, and D. G. Moore, 1981: Remote sensing of canopy temperature at incomplete cover. *Agron. J.* **73,** 403–406.

Henry, J. A., S. E. Dicks, O. F. Wetterqvist, and S. J. Roguski, 1989: Comparison of satellite, ground-based, and modeling techniques for analyzing the urban heat island. *Photogramm. Eng. Remote Sens.*, **55,** 69–76.

Jupp, D. L. B., J. Walker, and L. K. Penridge, 1986: Interpretation of vegetation structure in Landsat MSS imagery: A case study in disturbed semi-arid eucalypt woodland. Part 2. Model-based analysis. *J. Environ. Manag.*, **23,** 35–57.

Kneizys, F. X., E. P. Shettle, L. W. Abreu, J. H. Chetwynd Jr., G. P. Anderson, W. O. Gallery, J. E. A. Selby, and S. A. Clough, 1988: User's Guide to LOWTRAN 7. Air Force Geophysics Laboratory Rep. AFGL-TR-88-0177, 137 pp. [Available from Hanscom AFB, Air Force Geophysics Lab., Bedford, MA 01731.]

Kohsiek, W., H. A. R. de Bruin, H. The, and B. van den Hurk, 1993: Estimation of the sensible heat flux of a semi-arid area using surface radiative temperature measurements. *Bound.-Layer Meteor.*, **63,** 213–230.

Kramer, P. J., and T. T. Kozlowski, 1979: *Physiology of Woody Plants*. Academic Press, 811 pp.

Kustas, W. P., B. J. Choudhury, M. S. Moran, R. J. Reginato, R. D. Jackson, L. W. Gay, and H. L. Weaver, 1989: Determination of sensible hear flux over sparse canopy using thermal infrared data. *Agric. Forest Meteor.*, **44,** 197–216.

——, ——, Y. Inoue, P. J. Pinter, M. S. Moran, R. D. Jackson, and R. J. Reginato, 1990: Ground and aircraft infrared observations over a partially vegetated area. *Int. J. Remote Sens.*, **11,** 409–427.

Lang, A. R. G., and R. E. McMurtrie, 1992: Total leaf areas of single trees of *Eucalyptus grandis* estimated from transmittances of the sun's beam. *Agric. Forest Meteor.*, **58,** 79–92.

Lee, H.-Y., 1993: An application of NOAA AVHRR thermal data to the study of urban heat islands. *Atmos Environ.*, **27B,** 1–13.

Li, X., and A. H. Strahler, 1985: Geometrical-optical modelling of a conifer forest canopy. *IEEE Trans. Geosci. Remote Sens.*, **GE-23,** 705–721.

McGuire, M. J., L. K. Balick, J. A. Smith, and B. A. Hutchison, 1989: Modeling directional thermal radiance from a forest canopy. *Remote Sens. Environ.*, **27,** 169–186.

Nichol, J. E., 1996: High-resolution surface temperature patterns related to urban morphology in a tropical city: A satellite-based study. *J. Appl. Meteor.*, **35,** 135–146.

Norman, J. M., M. Divakarla, and N. S. Goel, 1995: Algorithms for extracting information from remote thermal-IR observations of the earth's surface. *Remote Sens. Environ.*, **51,** 157–168.

Paw U, K. T., 1992: Development of models for thermal infrared radiation above and within plant canopies. *ISPRS J. Photogramm. Remote Sens.*, **47,** 189–203.

Quattrochi, D. A., and M. K. Ridd, 1994: Measurement and analysis of thermal energy responses from discrete urban surfaces

using remote sensing data. *Int. J. Remote Sens.*, **15,** 1991–2022.

Roth, M., and T. R. Oke, 1993: Turbulent transfer relationships over an urban surface. I: Spectral characteristics. *Quart. J. Roy. Meteor. Soc.*, **119,** 1071–1104.

——, ——, and W. J. Emery, 1989: Satellite-derived urban heat islands from three coastal cities and the utilization of such data in urban climatology. *Int. J. Remote Sens.*, **10,** 1699–1720.

Schmid, H.-P., 1988: Spatial scales of sensible heat flux variability representativeness of flux measurements and surface layer structure over suburban terrain. Ph.D. thesis, University of British Columbia, 299 pp. [Available from the University of British Columbia Library, Special Collections, 1956 Main Mall, Vancouver, BC V6T 1Z1, Canada.]

Singh, S. M., 1985: Remarks on the use of a Stefan–Boltzmann-type relation for estimating surface temperatures. *Int. J. Remote Sens.*, **6,** 741–747.

Steyn, D. G., 1980: Turbulence, diffusion and the daytime mixed layer depth over a coastal city. Ph.D. thesis, University of British Columbia, 161 pp. [Available from The University of British Columbia Library, Special Collections, 1956 Main Mall, Vancouver, BC V6T 1Z1, Canada.]

Stoll, M. J., and A. J. Brazel, 1992: Surface-air temperature relationships in the urban environment of Phoenix, Arizona. *Phys. Geogr.,* **13,** 160–179.

Sun, J., and L. Mahrt, 1995: Relationship of surface heat flux to microscale temperature variations: Application to BOREAS. *Bound.-Layer Meteor.,* **76,** 291–301.

Vancouver Planning Department, 1984: Map of Downtown Building Heights [1:12000] City of Vancouver. [Available from the Vancouver Planning Dept., 453 West 12th Ave., Vancouver, BC V5Y 1V4, Canada.]

Voogt, J. A., 1995: Thermal remote sensing of urban surface temperatures. Ph.D. thesis, University of British Columbia, 340 pp. [Available from the University of British Columbia Library, Special Collections, 1956 Main Mall, Vancouver, BC V6T 1Z1, Canada.]

Willmott, C. J., 1981: On the validation of models. *Phys. Georgr.*, **2,** 184–194.